SECONDARY TEXTURES IN BRECCIATED BASALTIC EUCRITE MIL 11290. D. R. McQuaig[1, 2], T.J. Lapen[2], M. Righter[2], 1 Jacobs/JETS II, NASA-JSC (devin.r.mcquaig@nasa.gov), [2]Dept. of Earth and Atmospheric Sciences, University of Houston

Introduction: Basaltic eucrites originate from the upper crust of their parent body, likely asteroid 4-Vesta [1, 2]. This largely intact protoplanet has undergone differentiation and therefore provides insights into early planetary processes. Radiogenic chronometers indicate rapid planetary differentiation within <10 Ma of solar system formation and a period of magmatism spanning as much as 50 million years [3,4]. An extensive history of impacts prior to about 3.1 Ga significantly modified many materials derived from the eucrite parent body [5]. Therefore, eucrites display diverse igneous to metamorphic textures formed by endogenous crustal processes and impacts. Their mineralogy is dominantly composed of plagioclase, pigeonite, and augite with minor to accessory phases including silica, ilmenite, spinel, Ca-phosphates, olivine, zircon, Ni-poor metal, and potassium feldspar [2,6].

Although there are abundant achondrites originating from 4-Vesta, the geologic history of the body is not well understood. Better constraining the igneous textures and chemistry in basaltic eucrites are necessary to follow the magmatic evolution and impact history of this planetary body.

This study characterizes the composition, textures, and age of a basaltic eucrite through techniques such as electron microscopy, geochemistry, and geochronology to add to our understanding of early planetary formation.

Sample and Methods: An ~150 μm thick section and ~2.3 grams of intact pieces of MIL 11290 were allocated to this study through the Meteorite Working Group and NASA-JSC. Optical microscopy with reflective light was performed at the University of Houston (UH) while scanning electron microscopy (SEM) and electron probe analysis (EPMA) were performed at NASA-JSC on the JEOL 7600F and JEOL JXA-8350F, respectively. Inductively coupled plasma mass spectrometry was performed at UH using the multicollector (MC-ICP-MS) for isotopic analyses, laser ablation (LA-ICP-MS) for in-situ analyses, optical emission spectra (ICP-OES) for major and minor elements, and triple quadrapole (ICP-QQQ) for trace elements.

This work builds on the work presented in the Meteoritical Bulletin and within [7].

Results: *General Petrography*. MIL 11290, 10 consists of two lithologies and a brecciated zone between them. Lithology 1 consists of pyroxenes (46 vol%) and plagioclase (41 vol%) in sub-ophitic to ophitic texture with lesser amounts of silica (8%) and accessory minerals (4%) such as olivine, ilmenite, chromite, troilite, and Ca-phosphates. Most pyroxenes exhibit Fe-enrichment, sub-micron lamellae, high-Mg cores, and many contain veinlets of fayalitic olivine (Fig. 1). Plagioclase phases are mostly primary, indicating igneous crystallization. Secondary high-Ca plagioclase phases are inclusion free and minimally fractured (Fig. 2). They are associated with both types of olivine populations. Many of the minor phases, including silica polymorphs, are more concentrated in areas of mesostasis throughout the sample.

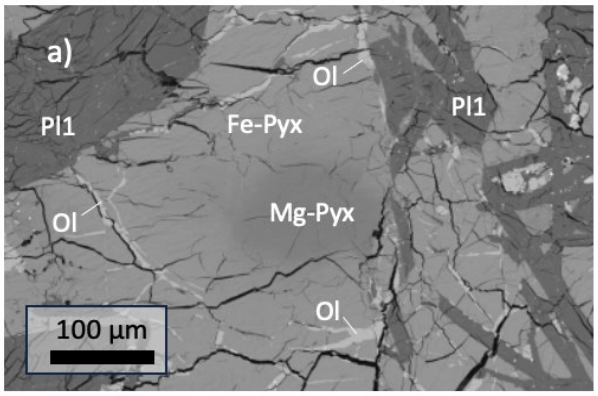

Figure 1. Backscattered electron image of lithology 1, MIL 11290, 10. Mg-Pyx: magnesium core of pigeonite. Fe-Pyx: iron enriched region surrounding the magnesium core. Ol: fayalitic olivine veinlets. Pl1: igneous plagioclase displaying fractures and inclusions.

Lithology 2 displays subophitic to ophitic textures with slightly different modal abundances than lithology 1. However, it is inevitable that some of the breccia zone was included in the point counting for lithology 2, so these numbers are to be taken with caution. Pyroxenes (44 vol%) display igneous zoning of high-Ca exsolution from the low-Ca core. Plagioclase (39 vol%) is fractured with subhedral to anhedral textures. This lithology also has areas of mesostasis containing silica (10 vol%) and accessory minerals (7%) of ilmenite and troilite. Olivine grains and chromite are absent, despite a careful search.

The brecciated zone contains mineralogies and textures representing both lithologies and recrystallized mineral phases. Minerals in this zone range from fine-grained minerals to medium grain sizes, intermixed. Areas within the breccia zone also contain secondary fayalitic olivine in monomineralic form. Both Fe-rich and zoned, igneous pyroxenes are found here in addition to igneous and secondary plagioclase phases. Mi-

nor and accessory minerals of silica, olivine, ilmenite, troilite, and Ca-phosphates are all found in the breccia zone, despite an absence of olivine in lithology 2 and troilite in lithology 1. A few small grains of chromite are present in throughout the sample. However, lithology 1 contains a larger grain (> 0.25 mm) of chromite.

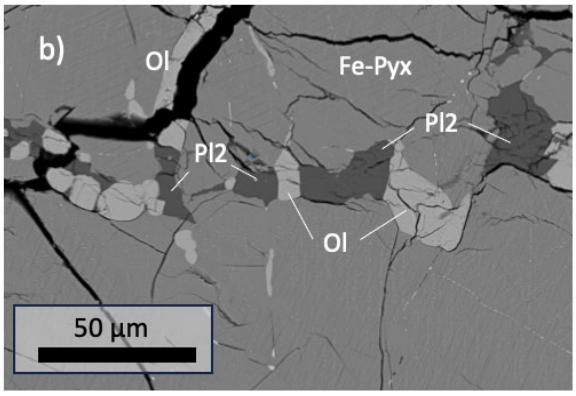

Figure 2. Backscattered electron image of Lithology 1, MIL 11290, 10. Fe-Pyx: iron enriched pigeonite with submicron lamellae visible. Ol: fayalitic olivine veinlets. Pl2: anorthitic, inclusion-free, secondary plagioclase.

Modal measurements of the entire thick section of MIL 11290,10 revealed abundances of pyroxene (47 vol%), plagioclase (40 vol%), silica (9 vol%), and accessory minerals (ilmenite, Ca-phosphate, chromite, troilite, and olivine). Lithologies 1 and 2 differ slightly, with Lithology 2 containing more silica and accessory phases (2% more and 3% more, respectively) while Lithology 1 has a 2 vol% higher abundance of pyroxene and plagioclase.

In addition to modal differences, the grain sizes are typically larger in lithology 1. On average, plagioclase grains are 0.65 mm x 0.21 mm in lithology 1 versus 0.55 mm x 0.12 mm in lithology 2. Average pyroxene sizes, however, are doubled in length in lithology 1 (1.00 mm x 0.35 mm) compared to 0.56 mm x 0.30 mm in lithology 2. A few small grains of chromite (< 10 µm) are present throughout the sample. However, lithology 1 contains a larger grain (> 40 µm) of chromite.

Post-crystallization processes such as annealing and brecciation are common in eucrites. However, many studies have also noted igneous pyroxenes that are Fe-rich, leaving igneous, high-Mg cores. Secondary fayalitic olivine veinlets (Fa 64-70), pyroxene, anorthite (An 97-99), sometimes accompanied by minor amounts of troilite or Cr-spinel [e.g., 8-15].

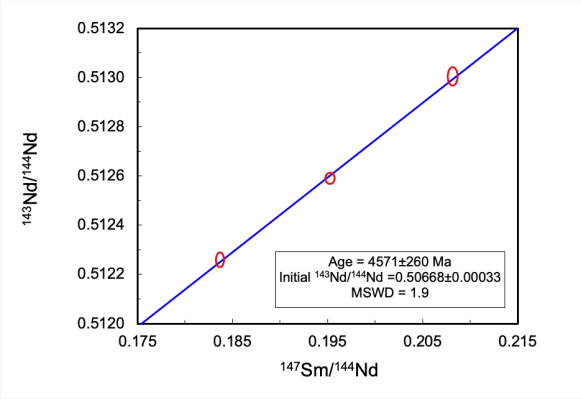

Figure 3. Isochron plot of $^{143}Nd/^{144}Nd$ ratio vs $^{147}Sm/^{144}Nd$. Indicating a potential crystallization age of 4571 ± 240 Ma (MSWD = 1.9).

Discussion: In this study, petrological, geochemical, and chronological investigations were performed on basaltic eucrite MIL 11290. Chemical compositions and distinct textural differences between lithology 1 and lithology 2 indicate that this sample is a polymict eucrite with secondary Fe-enrichment of lithology 1. The igneous zoning with submicron exsolution lamellae of high-Ca pyroxene from low-Ca pyroxene designate a metamorphic grade of type 3. Fe/Mn ratios of 28-32 are consistent with the HED clan as originating from the same parent body, aside from some anomalous eucrite-like samples. REE patterns normalized to CI chondritic values are relatively flat, though slightly more enriched than the representative lithology in Juvinas for the Main Group. However, initial bulk measurements assumed that this rock was unbrecciated and we now think that lithologies 1 and 2 may represent both a Main Group and a Nuevo Laredo group eucrite. The $^{147}Sm/^{144}Nd$ isochron for MIL 11290 yields an age of 4571 ± 240 Ma, indicating an initial age of crystallization for this sample. Further, the results suggest that lithology 1 of MIL 11290 experienced secondary Fe-enrichment while in situ before the subsequent impact of lithology 2, evidenced by only igneous textures in lithology 2 and a lack of iron redistribution.

References: [1] Scott E.R.D. et al. (2009) *GCA 73*, 5835. [2] Mittlefehldt D.W. (2015) *Chemie der Erde-Geochemistry 75*, 55. [3] Schiller M. et al. (2010) *GCA* 74, 4844. [4] Touboul M. et al. (2015) *GCA 156*, 106 [5] Bogard D. and Garrison D. (2003) *MAPS 38*, 669. [6] McQuaig, D.R. (2019) *LPSC L,* Abstract #3000. [7] Mittlefehldt D.W. et al. (2021) *MAPS 57*, 484-526. [8] Takeda H. and Graham A.L. (1991) *Meteoritics 26*, 129-134. [9] Mittlefehldt and Lindstrom (1997) *GCA 61*, 453-462. [10] Warren P.H. (2002) *LPSC XXXIII*

Abstract #1147. [11] Barrat J.A. et al. (2011) *GCA 75*, 3839-3852. [12] Roszjar J. et al. (2011) *MAPS 46,* 1754-1773. [13] Warren P.H. et al. (2014) *GCA 141,* 199-227. [14] Vollmer C. et al (2020) *MAPS 55,* 558-574. [15] Shisseh T. et al. (2023) *GCA 340*, 51-64.